Reverse circular Bragg phenomenon

Martin W. McCall [*] and Stefanos Fr. Koufidis [†]
Blackett Laboratory, Department of Physics, Imperial College of Science, Technology and Medicine, Prince Consort Road, London SW7 2AZ, United Kingdom

(Received 30 September 2022; revised 3 November 2022; accepted 14 November 2022; published 30 November 2022)

The problem of axial propagation of circularly polarized light in a circularly birefringent structurally chiral medium is exactly solved via full electromagnetic analysis. Underlying symmetries of the system's characteristic matrix reveal interesting insights, which are confirmed by coupled wave theory. For extreme values of chirality, a reverse circular Bragg resonance arises in the negative refraction regime where handedness reversal of counterpart modes occurs. A condition is identified under which circular birefringence precisely offsets structural chirality, rendering the medium simply linearly birefringent. Manufacturing such a medium is feasible via current metamedia and inorganic materials technology and has applications in optics, optoelectronics, and sensing.

DOI: 10.1103/PhysRevResearch.4.043154

I. INTRODUCTION

Chirality, or the geometric property that an object cannot be superimposed with its mirror image, is pervasive in nature [1], and was recently studied in artificial metamedia for its potential applications in optoelectronics [2] and sensing [3]. The electromagnetic response of chiral media has two distinct origins. The first is via magnetoelectric coupling, which in natural media arises from chirality at the molecular scale. The characteristic response of this form of chirality is optical rotation, whereby the plane of linearly polarized light is rotated on transmission, or, equivalently, circular birefringence, whereby right and left circular polarizations (RCP and LCP, respectively) propagate at different speeds. On optical rotation, we note that electric-dipole–electric-quadrupole coupling also exists, with its contribution becoming comparable to the magnetoelectric coupling in natural Rayleigh or Raman optical activity [4]. The other origin of electromagnetic chirality is via helical stacking of birefringent layers in structurally chiral media, such as cholesteric liquid crystals [5] or sculptured thin films [6]. Their signature response is the circular Bragg phenomenon, wherein cohanded polarized light effectively experiences a periodic modulation of the refractive index by alternately sampling the two refractive indices associated with the two orthogonal axes, progressively rotating along the direction of propagation. Then, monochromatic light is strongly reflected when its wavelength in the medium matches the helical pitch, the so-called Bragg condition. On the other hand, the propagation of contrahanded polarized light, whose helicity is opposite to the medium's spatial handedness, is unaffected, seeing an average refractive index.

How to optically characterize media with either form of chirality was discussed in Ref. [7], and the differentiation between structural and molecular chirality was recently explained in the context of polymer thin films in Ref. [8]. Either or both forms of chirality represent opportunities for manipulation of circularly polarized light, which is attracting increasing attention in modern optoelectronics [9]. Such polarization selectivity can, e.g., enhance the throughput efficiency of organic light-emitting diode (OLED) displays [10] or enhance spin polarized electron transport in chiral organic semiconductors [11]. Although the interaction of light with naturally chiral media is typically weak, recent advances in metamedia fabrication have augmented the chiroptical response [12]. In particular, a "curled" metasurface with giant chirality was experimentally demonstrated in Ref. [13], while in Ref. [14], it was shown that incrementing the metasurface area significantly enhances optical activity.

The asymmetrical response of structurally chiral media was studied in Refs. [15–19], where the problem of axial propagation was exactly solved via full electromagnetic analysis and approximately via coupled wave theory. The location of the Bragg resonances is sensitive to various parameters and plays an important role in many applications in sensing [20]. Indeed, in Ref. [21], the increment of the volumetric fraction shifted the Bragg resonance towards the blue, and an experiment conducted in Ref. [22] found a similar blue-shifting with increment of the deposition angle [18]. Two opposite-sign lateral shifts at the edges of the Bragg zone of a nanocomposite structurally chiral medium were seen in Ref. [23], and in Ref. [24] a shift towards shorter wavelengths was associated with material changes occurring during annealing. The porosity of structurally chiral media offers a platform for fluid infiltration, and a spectral shift, strongly dependent on the fluid's refractive index, was demonstrated in Ref. [25]. This extended the work in Ref. [26], which found that infiltration of void regions with a higher-refractive-index material enhanced

[*] m.mccall@imperial.ac.uk
[†] steven.koufidis20@imperial.ac.uk

optical activity, which is approximately proportional to the square of the local linear birefringence [27].

A natural question to address is the electromagnetic response of a medium that combines both structural and magnetoelectric chirality. This appears to have been first examined numerically in Refs. [28,29], where the optical response of a chiral sculptured thin film, infiltrated by an isotropic chiral fluid, was studied. Apparently, the chiral fluid shifts the optical spectrum, linearly to its chirality, also affecting the peak reflectance and bandwidth. In this paper, the axial propagation of circularly polarized light in a circularly birefringent structurally chiral medium is solved analytically, and identification of some of the system's underlying symmetries reveals significant insights. In particular, we demonstrate that additional resonances compared with those demonstrated in Refs. [28,29] occur, as in Refs. [30,31], but in a different kind of material-light interaction. When the optical rotatory power is extreme, eliciting negative refraction due to chirality (as was theoretically predicted in Refs. [32,33] and experimentally realized in Refs. [34–36]), the handedness and phase velocity of counterpart modes interchange. This reverse circular Bragg phenomenon is related to metamaterials with giant optical activity [37] and is fundamentally distinct from the handedness reversal phenomenon due to the permittivity and permeability being simultaneously negative that was found in Ref. [38]. Furthermore, chiral inorganic nanomaterials exhibiting enough chirality so that the refractive index associated with one polarization becomes negative [39] are preferable candidates for small-volume and low-energy-consumption practical realizations of the proposed medium.

The paper is organized as follows: In Sec. II, constitutive relations for circularly birefringent structurally chiral media are formed, and in Sec. III the problem of axial propagation is exactly solved via full electromagnetic analysis. In Sec. IV the optical response of a slab of the considered medium is investigated and the aforementioned resonances are demonstrated. Finally, a condition under which circular birefringence precisely offsets structural chirality, rendering the medium simply linearly birefringent, is identified in Sec. V. Conclusions are given in Sec. VI. The handedness reversal of counterpropagating modes in the negative refraction regime is reviewed in Appendix A, and coupled wave theory, applied to corroborate the theoretical predictions, is summarized in Appendix B.

II. CONSTITUTIVE RELATIONS

A. Circularly birefringent media

According to the Drude-Born-Fedorov model [40], the temporal frequency domain constitutive relations for optical activity in a bi-isotropic reciprocal medium are

$$\mathbf{D} = \varepsilon_0(\varepsilon\mathbf{E} + i\alpha\eta_0\mathbf{H}), \tag{1}$$

$$\mathbf{B} = \mu_0[-i(\alpha/\eta_0)\mathbf{E} + \mu\mathbf{H}]. \tag{2}$$

Here, $\mathbf{E}$, $\mathbf{B}$ are the fundamental electromagnetic fields and $\mathbf{D}$, $\mathbf{H}$ are the excitation fields. The free-space permittivity, permeability, and impedance are ε_0, μ_0, and $\eta_0 = (\mu_0/\varepsilon_0)^{1/2}$, respectively, the relative permittivity is ε, and the relative permeability is μ. The chirality parameter $\alpha \in \mathbb{R}$ measures the distance (in wavelengths) after which the $\mathbf{E}$ vector of a linearly polarized wave completes a full rotation. Defining the auxiliary fields $\mathbf{h} = \eta_0\mathbf{H}$, $\mathbf{b} = (\eta_0/\mu_0)\mathbf{B}$, and $\mathbf{d} = \varepsilon_0^{-1}\mathbf{D}$, with the same dimensions as $\mathbf{E}$, Eqs. (1) and (2) become

$$\mathbf{d} = \varepsilon\mathbf{E} + i\alpha\mathbf{h},$$
$$\mathbf{b} = -i\alpha\mathbf{E} + \mu\mathbf{h},$$

respectively. Maxwell's macroscopic source-free curl relations, under the $\exp(-i\omega t)$ harmonic convention, are written as

$$\nabla \times \mathbf{E} = k_0\alpha\mathbf{E} + ik_0\mu\mathbf{h}, \tag{3}$$

$$\nabla \times \mathbf{h} = -ik_0\varepsilon\mathbf{E} + k_0\alpha\mathbf{h}, \tag{4}$$

where $k_0 = (\varepsilon_0\mu_0)^{1/2}\omega$ is the free-space wave number. For plane wave propagation along z, with a unit vector $\hat{\mathbf{z}}$, combining Eqs. (3) and (4) yields

$$\frac{d^2\mathbf{E}}{dz^2} + 2\alpha k_0\frac{d}{dz}(\hat{\mathbf{z}} \times \mathbf{E}) + k_0^2(\mu\varepsilon - \alpha^2)\mathbf{E} = \mathbf{0}, \tag{5}$$

which is the Helmholtz wave equation describing axial propagation in isotropic circularly birefringent media.

B. Structurally chiral media

A structurally chiral medium is modeled by a dielectric tensor of the form

$$\boldsymbol{\epsilon} = \boldsymbol{\mathcal{R}} \cdot \hat{\boldsymbol{\epsilon}} \cdot \boldsymbol{\mathcal{R}}^{-1},$$

where $\hat{\boldsymbol{\epsilon}}$ is the background (i.e., static) dielectric tensor, and in Cartesian coordinates,

$$\boldsymbol{\mathcal{R}} = \begin{pmatrix} \cos(pz) & -h\sin(pz) & 0 \\ h\sin(pz) & \cos(pz) & 0 \\ 0 & 0 & 1 \end{pmatrix}$$

describes the periodic rotation of the eigenaxes of $\boldsymbol{\epsilon}$ along and about the z axis with a spatial period $L_p = 2\pi/p$ [19]. For $h = +1$, the eigenaxes of $\boldsymbol{\epsilon}$ rotate in a right-handed (RH) sense, while for $h = -1$, the rotation is regarded as left-handed (LH). The transverse projection of $\boldsymbol{\mathcal{R}}$ can be expressed as [15]

$$\boldsymbol{\mathcal{R}}_\perp = \tfrac{1}{2}\boldsymbol{\sigma}e^{ipz} + \tfrac{1}{2}\boldsymbol{\sigma}^* e^{-ipz}, \tag{6}$$

where

$$\boldsymbol{\sigma} = \begin{pmatrix} 1 & hi \\ -hi & 1 \end{pmatrix}.$$

Denoting as $\boldsymbol{\epsilon}_{\text{ref}}$ the reference tensor, with Cartesian components $\boldsymbol{\epsilon}_{\text{ref}} = \text{diag}(\varepsilon_a, \varepsilon_b, \varepsilon_c)$, the background tensor accounts for the orientation of the principal axes as

$$\hat{\boldsymbol{\epsilon}} = \boldsymbol{\chi} \cdot \boldsymbol{\epsilon}_{\text{ref}} \cdot \boldsymbol{\chi}^{-1},$$

where

$$\boldsymbol{\chi} = \begin{pmatrix} \cos\chi & 0 & -\sin\chi \\ 0 & 1 & 0 \\ \sin\chi & 0 & \cos\chi \end{pmatrix},$$

and the so-called rise angle χ tilts the eigenaxes in the x-z plane. It is straightforward to show that the projection of $\hat{\boldsymbol{\epsilon}}$ in

the x-y plane takes the diagonal form [19]

$$\hat{\boldsymbol{\epsilon}}_\perp = \begin{pmatrix} \widetilde{\varepsilon} & 0 \\ 0 & \varepsilon_b \end{pmatrix}, \tag{7}$$

where

$$\widetilde{\varepsilon} = \frac{\varepsilon_a \varepsilon_c}{\varepsilon_a \sin^2\chi + \varepsilon_c \cos^2\chi}.$$

It is convenient to reexpress the tensor of Eq. (7) as

$$\hat{\boldsymbol{\epsilon}}_\perp = \bar{\varepsilon}\,\mathbb{I} + \delta\varepsilon\,\mathbb{J},$$

where

$$\bar{\varepsilon} = (\widetilde{\varepsilon} + \varepsilon_b)/2, \quad \delta\varepsilon = (\widetilde{\varepsilon} - \varepsilon_b)/2, \tag{8}$$

$\mathbb{I}$ is the 2×2 identity, and $\mathbb{J} = \mathrm{diag}(1, -1)$. Overall,

$$\boldsymbol{\epsilon}_\perp(z, h) = \boldsymbol{\mathcal{R}}_\perp \cdot \hat{\boldsymbol{\epsilon}}_\perp \cdot \boldsymbol{\mathcal{R}}_\perp^{-1} \tag{9}$$

is the z-dependent tensor describing structural chirality, which also depends on the medium's spatial handedness h.

C. Circularly birefringent structurally chiral media

As we are interested in axial propagation in an anisotropic medium that combines circular birefringence with structural chirality, the scalar ε appearing in Eq. (5), for the transverse component of the electric field $\mathbf{E}_\perp$, is replaced by the tensor $\boldsymbol{\epsilon}_\perp$ of Eq. (9), presumed to be inhomogeneous along the z direction only. Such a Helmholtz wave equation shall be describing axial propagation in circularly birefringent structurally chiral media.

III. FULL ELECTROMAGNETIC ANALYSIS FOR AXIAL PROPAGATION

Considering the transverse components of the fields, Eqs. (3) and (4) can be written in a matrix notation as

$$\frac{d}{dz}(\times)\begin{pmatrix} \mathbf{E}_\perp \\ \mathbf{h}_\perp \end{pmatrix} = ik_0 \begin{pmatrix} -i\alpha\mathbb{I} & \mu\mathbb{I} \\ -\boldsymbol{\epsilon}_\perp & -i\alpha\mathbb{I} \end{pmatrix}\begin{pmatrix} \mathbf{E}_\perp \\ \mathbf{h}_\perp \end{pmatrix}, \tag{10}$$

where $(\times)$ has Cartesian components $\left(\begin{smallmatrix} 0 & -1 \\ 1 & 0 \end{smallmatrix}\right)$ and acts on both $\mathbf{E}_\perp$ and $\mathbf{h}_\perp$. The system of Eq. (10) can be rendered autonomous via the Oseen transformation [41]

$$\mathbf{e} = \boldsymbol{\mathcal{R}}_\perp^{-1} \cdot \mathbf{E}_\perp, \tag{11a}$$

$$\widetilde{\mathbf{h}} = \boldsymbol{\mathcal{R}}_\perp^{-1} \cdot \mathbf{h}_\perp, \tag{11b}$$

under the convention of Ref. [42]. Via Eqs. (11a) and (11b), the two lines of the system in Eq. (10) become

$$\frac{d}{dz}(\times)\mathbf{e} = -\boldsymbol{\mathcal{R}}_\perp^{-1}\frac{d\boldsymbol{\mathcal{R}}_\perp}{dz}(\times)\mathbf{e} + \alpha k_0 \mathbf{e} + ik_0\mu\widetilde{\mathbf{h}},$$

$$\frac{d}{dz}(\times)\widetilde{\mathbf{h}} = -\boldsymbol{\mathcal{R}}^{-1}\frac{d\boldsymbol{\mathcal{R}}_\perp}{dz}(\times)\widetilde{\mathbf{h}} - ik_0\hat{\boldsymbol{\epsilon}}_\perp \cdot \mathbf{e} + \alpha k_0 \widetilde{\mathbf{h}},$$

and it is easy to show that they can be simplified to

$$\frac{d}{dz}\begin{pmatrix} \mathbf{e} \\ \widetilde{\mathbf{h}} \end{pmatrix} = (\times)\begin{pmatrix} -hp - k_0\alpha & -ik_0\mu \\ ik_0\hat{\boldsymbol{\epsilon}}_\perp & -hp - k_0\alpha \end{pmatrix}\begin{pmatrix} \mathbf{e} \\ \widetilde{\mathbf{h}} \end{pmatrix}. \tag{12}$$

In terms of the $\mathbf{G} = (e_x,\ e_y,\ \widetilde{h}_x,\ \widetilde{h}_y)^T$ components of the Oseen-transformed fields, where T denotes transpose,

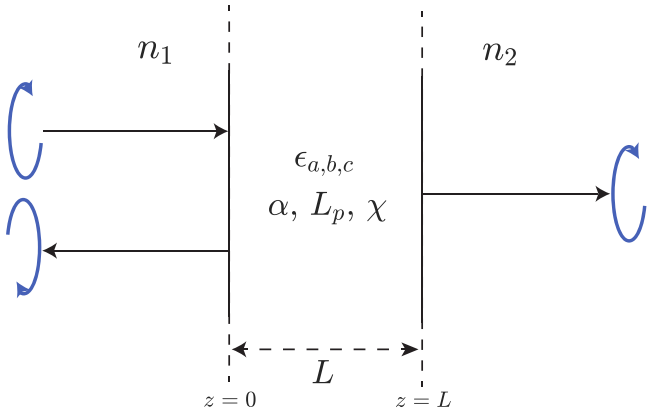

FIG. 1. A length $L = 6\,\mu$m slab of a right-handed ($h = +1$) circularly birefringent structurally chiral medium, stacked between two non-index-matched isotropic dielectrics with refractive indices $n_1 = 1$ and $n_2 = 2$. Light is normally incident and the arrows indicate the incident, reflected, and transmitted circular polarizations. The medium's base parameters are $\varepsilon_a = 3.2 + 0.02i$, $\varepsilon_b = 2.9 + 0.02i$, $\varepsilon_c = 2.8 + 0.02i$, $\mu = 1$, $L_p = 300$ nm, and $\chi = 30^\circ$.

Eq. (12) can be equivalently written in the vectorial-differential form

$$\frac{d\mathbf{G}}{dz} = \mathbf{F} \cdot \mathbf{G}, \tag{13}$$

where the components of the characteristic matrix are

$$\mathbf{F} = \begin{pmatrix} 0 & hp + k_0\alpha & 0 & ik_0\mu \\ -hp - k_0\alpha & 0 & -ik_0\mu & 0 \\ 0 & -ik_0\epsilon_b & 0 & hp + k_0\alpha \\ ik_0\tilde{\epsilon} & 0 & -hp - k_0\alpha & 0 \end{pmatrix}. \tag{14}$$

The exact solution to the autonomous system of Eq. (13) can be used to construct the axially propagating fields via Eqs. (11a) and (11b), from which the reflection and transmission coefficients of polarized light incident to a slab of the considered medium may be computed. Indeed, assuming a slab extended between $z = 0$ and $z = L$, as illustrated in Fig. 1, the solution to Eq. (13) for the transverse components of the fields is [19]

$$\begin{pmatrix} \mathbf{E}_\perp \\ \mathbf{h}_\perp \end{pmatrix}_{z=L} = \begin{pmatrix} \boldsymbol{\mathcal{R}}_\perp & \mathbf{0} \\ \mathbf{0} & \boldsymbol{\mathcal{R}}_\perp \end{pmatrix} e^{\mathbf{F}L}\begin{pmatrix} \mathbf{E}_\perp \\ \mathbf{h}_\perp \end{pmatrix}_{z=0},$$

where $\mathbf{0}$ is the 2×2 null matrix and $e^{\mathbf{F}L}$ is a well-defined matrix exponential. For $a_{x,y}$, $r_{x,y}$, and $t_{x,y}$ being the amplitudes of the incident, reflected, and transmitted electric fields in Cartesian coordinates, respectively, field matching at both interfaces of Fig. 1 requires

$$\begin{pmatrix} \mathbf{E}_\perp \\ \mathbf{h}_\perp \end{pmatrix}_{z=0} = \begin{pmatrix} a_x + r_x \\ a_y + r_y \\ -n_1(a_y - r_y) \\ n_1(a_x - r_x) \end{pmatrix},$$

$$\begin{pmatrix} \mathbf{E}_\perp \\ \mathbf{h}_\perp \end{pmatrix}_{z=L} = \begin{pmatrix} t_x \\ t_y \\ -n_2 t_y \\ n_2 t_x \end{pmatrix}.$$

The linear reflection and transmission coefficients are defined as

$$\begin{pmatrix} r_x \\ r_y \end{pmatrix} = \begin{pmatrix} r_{xx} & r_{xy} \\ r_{yx} & r_{yy} \end{pmatrix} \begin{pmatrix} a_x \\ a_y \end{pmatrix},$$
$$\begin{pmatrix} t_x \\ t_y \end{pmatrix} = \begin{pmatrix} t_{xx} & t_{xy} \\ t_{yx} & t_{yy} \end{pmatrix} \begin{pmatrix} a_x \\ a_y \end{pmatrix},$$

respectively, and converting to a circular basis yields

$$\begin{pmatrix} r_{LL} & r_{LR} \\ r_{RL} & r_{RR} \end{pmatrix} = \frac{1}{2} \begin{pmatrix} 1 & i \\ 1 & -i \end{pmatrix} \begin{pmatrix} r_{xx} & r_{xy} \\ r_{yx} & r_{yy} \end{pmatrix} \begin{pmatrix} 1 & 1 \\ i & -i \end{pmatrix},$$
$$\begin{pmatrix} t_{LL} & t_{LR} \\ t_{RL} & t_{RR} \end{pmatrix} = \frac{1}{2} \begin{pmatrix} 1 & -i \\ 1 & i \end{pmatrix} \begin{pmatrix} t_{xx} & t_{xy} \\ t_{yx} & t_{yy} \end{pmatrix} \begin{pmatrix} 1 & 1 \\ i & -i \end{pmatrix}.$$

The intensity reflectances are then $R_{i,j} = |r_{i,j}|^2$, while the intensity transmittances $T_{i,j} = (n_2/n_1)|t_{i,j}|^2$, with $\{i, j\} = \{R, L\}$ indicating reflection or transmission of the i polarization for incident j polarization.

IV. OPTICAL RESPONSE

A. Regular circular Bragg phenomenon

In the absence of circular birefringence, $\alpha = 0$ and the characteristic matrix $\mathbf{F}$ of Eq. (14) describes axial propagation through a usual structurally chiral medium. It is well established that the resulting optical spectrum shows the circular Bragg phenomenon if the condition $\lambda_0^{\rm Br} = {\rm Re}(\bar{n})L_p$, where $\bar{n} = (\bar{\varepsilon}\mu)^{1/2}$ with $\bar{\varepsilon}$ defined in Eq. (8), is met. In this instance, circularly polarized light that is cohanded with the medium will be strongly reflected, whereas contrahanded light will be transmitted (see, e.g., Refs. [15,16,19,42]).

If the structurally chiral medium is now infiltrated by a chiral fluid, i.e., if $\alpha \neq 0$, it will also become circularly birefringent. From Eqs. (13) and (14), it is evident that combining circular birefringence with structural chirality is mathematically described by a *linear perturbation* to the characteristic matrix of a simple uninfiltrated structurally chiral medium (cf. Eq. (14) for $\alpha = 0$ and $p = p'$), namely,

$$p' \to p + (\alpha/h)k_0. \tag{15}$$

In a circularly birefringent structurally chiral medium, the perturbation of Eq. (15) will result in a shift of the Bragg wavelength determined from

$$\left(\lambda_0^{\rm Br}\right)' = \frac{2\pi}{p'}{\rm Re}(\bar{n}) = \frac{2\pi\,{\rm Re}(\bar{n})}{p + (\alpha/h)\left[2\pi/\left(\lambda_0^{\rm Br}\right)'\right]},$$

where solving for $(\lambda_0^{\rm Br})'$ yields

$$\left(\lambda_0^{\rm Br}\right)' = L_p[{\rm Re}(\bar{n}) - \alpha/h]. \tag{16}$$

Hence setting $h = +1$ for a right-handed medium, RCP light will be resonant at

$$\lambda_0^{\rm Br}\big|_{\rm RH}^{\rm RCP} = L_p[{\rm Re}(\bar{n}) - \alpha], \quad \alpha < {\rm Re}(\bar{n}), \tag{17}$$

whereas in a left-handed medium, $h = -1$ and LCP light will be resonant at

$$\lambda_0^{\rm Br}\big|_{\rm LH}^{\rm LCP} = L_p[{\rm Re}(\bar{n}) + \alpha], \quad \alpha > -{\rm Re}(\bar{n}), \tag{18}$$

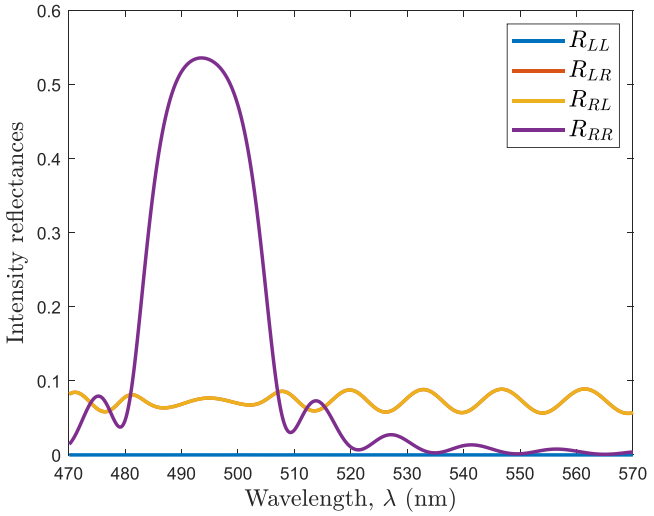

FIG. 2. Intensity reflectances of the setup in Fig. 1 for a physical value of chirality, $\alpha = 0.084$. The contrahanded reflectances R_{LR} and R_{RL} coincide.

where we have also stated the conditions that α and $\bar{n}$ must satisfy so that the wavelengths remain positive. These considerations quantitatively explain the spectral shifts observed numerically in Refs. [28,29], since our system in Eq. (13) is a special case of Eq. (18) in Ref. [28] describing infiltration by a general anisotropic chiral fluid.

To demonstrate these resonances, we consider a sculptured thin film, whose porous nature makes it ideal to be infiltrated by a chiral fluid, e.g., the D-glucose solution $C_6H_{12}O_6 \cdot H_2O$. In Ref. [43], the real part of the specific chirality of such a solution is $[\alpha] \approx 1.37 \times 10^{-6}$ cm^3/g, while the imaginary part is almost zero (at 21.5 °C). For a concentration close to saturation $C = 1.8$ g/cm^3, the chirality parameter is $\alpha = 2.46 \times 10^{-6}$. For the purpose of demonstration, we set $\alpha = 0.084$, which is a reasonably high but not extreme value (almost six times lower than the chirality value used in Ref. [28]), lying within $-\bar{n} < \alpha < \bar{n}$. The intensity reflectances and transmittances, for the setup in Fig. 1, can be seen in Figs. 2 and 3,

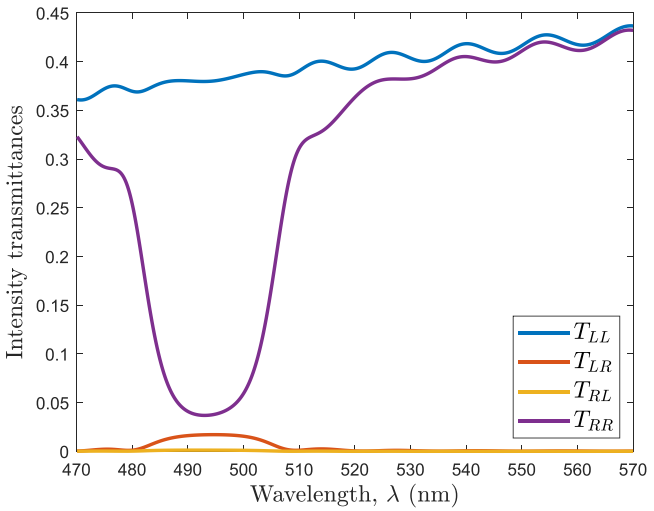

FIG. 3. Intensity transmittances for the scenario of Fig. 2.

respectively. We note that in the presence of absorption, the transmittance responds asymmetrically to the reflectance and the $R + T = 1$ condition no longer holds.

Evidently, circularly birefringent structurally chiral media exhibit a circular Bragg phenomenon for cohanded polarized light. In the absence of circular birefringence the central Bragg wavelength would be $\lambda_0^{\rm Br} = 519.1$ nm, while in its presence, it is shifted towards the blue at $(\lambda_0^{\rm Br})' = 493.9$ nm for a right-handed medium, as per Eq. (17), or towards the red at $(\lambda_0^{\rm Br})'' = 544.3$ nm for a left-handed one, as per Eq. (18), by $|\delta\lambda| = |L_p\alpha| = 25.2$ nm. This spectral shift characterizes both the medium and the chiral fluid, offering a platform for sensing either the concentration or the specific chirality of solutions [20].

B. Reverse circular Bragg phenomenon

The characteristic matrix of Eq. (14) is generally a function of the medium's parameters $\mathbf{F} \equiv \mathbf{F}(\varepsilon_b, \tilde{\varepsilon}, \mu; k_0; p, h, \alpha)$. Working explicitly in the $|\alpha| > \mathrm{Re}(\bar{n})$ regime, by performing the transformation

$$(\varepsilon_b, \tilde{\varepsilon}, \mu; k_0; p, h, \alpha) \to (\varepsilon_b, \tilde{\varepsilon}, \mu; k_0; -p, h, -\alpha), \tag{19}$$

so that the perturbation of Eq. (15) becomes $p' \to -p - (\alpha/h)k_0$, we effectively reverse the handedness via p and not via h, which is fixed for a particular medium. For ε_b, $\tilde{\varepsilon}$, and μ unchanged, it turns out that an underlying symmetry of the characteristic matrix $\mathbf{F}$ is

$$\mathbf{F}(p, h, \alpha) = \boldsymbol{\mathcal{H}} \cdot \mathbf{F}(-p, h, -\alpha) \cdot \boldsymbol{\mathcal{H}}, \tag{20}$$

where $\boldsymbol{\mathcal{H}} = \mathrm{diag}(1, -1, -1, 1)$, with $\boldsymbol{\mathcal{H}}^{-1} = \boldsymbol{\mathcal{H}}$. We now return to Eq. (13), which via Eq. (20) is written as

$$\frac{d[\mathbf{G}(p, h, \alpha)]}{dz} = [\boldsymbol{\mathcal{H}} \cdot \mathbf{F}(-p, h, -\alpha) \cdot \boldsymbol{\mathcal{H}}] \cdot \mathbf{G}(p, h, \alpha)$$

and implies that

$$\mathbf{G}(p, h, \alpha) = \boldsymbol{\mathcal{H}} \cdot \mathbf{G}(-p, h, -\alpha). \tag{21}$$

Such symmetry entails that

$$\{a_L \leftrightarrow a_R,\ r_L \leftrightarrow r_R,\ t_L \leftrightarrow t_R\}, \tag{22}$$

according to Eq. (18) of Ref. [38], meaning that the indices of the reflection and transmission coefficients are interchanged ($R \leftrightarrow L$). Then, nominally RCP light will become LCP and vice versa. Thus the transformation of Eq. (19) creates the illusion that the medium's handedness is reversed, although h is fixed.

To provide a firmer explanation of Eq. (22), we may examine the modes supported by a purely circularly birefringent medium. As discussed in Appendix A, for $|\alpha| < \mathrm{Re}(\bar{n})$, the forward propagating eigenmodes have field vectors that trace both left- and right-handed spatial helices (cf. Eqs. (A2) and (A3), respectively). For $|\alpha| > \mathrm{Re}(\bar{n})$, if we apply the transformation of Eq. (19) to the real part of the nominally forward propagating RCP electric field, it is straightforward to show that both the direction of propagation and the handedness of the mode reverse. That is, the handedness of the cohanded forward propagating mode swaps with the handedness of the contrahanded backward propagating one. Indeed, for $\alpha \to -\alpha$ and $p \to -p$, the handedness is reversed,

$$\begin{pmatrix} \cos[k_0(\mathrm{Re}(\bar{n}) - \alpha)z] \\ \sin[k_0(\mathrm{Re}(\bar{n}) - \alpha)z] \end{pmatrix} \to \begin{pmatrix} \cos[k_0(\mathrm{Re}(\bar{n}) + \alpha)z] \\ -\sin[k_0(\mathrm{Re}(\bar{n}) + \alpha)z] \end{pmatrix},$$

since on-resonance, the wave number transforms as $k_0 = p/(\mathrm{Re}(\bar{n}) - \alpha) \to -p/(\mathrm{Re}(\bar{n}) + \alpha)$.

If we apply the transformation of Eq. (19) to the general expression of the shifted Bragg wavelength in Eq. (16), we obtain

$$\left(\lambda_0^{\rm Br}\right)' = \frac{2\pi}{p'}\mathrm{Re}(\bar{n}) = \frac{2\pi\,\mathrm{Re}(\bar{n})}{-p - (\alpha/h)\left[2\pi/\left(\lambda_0^{\rm Br}\right)'\right]},$$

where solving for $(\lambda_0^{\rm Br})'$ yields

$$\left(\lambda_0^{\rm Br}\right)' = -L_p[\mathrm{Re}(\bar{n}) + \alpha/h], \tag{23}$$

which is obviously Eq. (16) for $\alpha \to -\alpha$ and $p \to -p$.

With the polarization states reversed, the resulting resonance in a right-handed medium for LCP light is at

$$\lambda_0^{\rm Br}\big|_{\rm RH}^{\rm LCP} = -L_p[\mathrm{Re}(\bar{n}) + \alpha], \quad \alpha < -\mathrm{Re}(\bar{n}), \tag{24}$$

while in a left-handed medium, for RCP light, it is at

$$\lambda_0^{\rm Br}\big|_{\rm LH}^{\rm RCP} = -L_p[\mathrm{Re}(\bar{n}) - \alpha], \quad \alpha > \mathrm{Re}(\bar{n}). \tag{25}$$

Remarkably, in a right-handed medium, the condition for the resonance occurrence in Eq. (17), $\alpha < \mathrm{Re}(\bar{n})$, is *still satisfied* when the condition of Eq. (24) is met. Consequently, for $\alpha < -\mathrm{Re}(\bar{n})$, two resonances are expected: one corresponding to light that is cohanded with the medium being reflected and another resonance, unforeseen, that backscatters light that is nominally contrahanded with the medium. Similarly, for a left-handed medium the condition of Eq. (25), $\alpha > \mathrm{Re}(\bar{n})$, simultaneously satisfies the condition of Eq. (18). This backscatters RCP light in a left-handed medium. These resonances are signatures of a *reverse circular Bragg phenomenon*.

For the setup in Fig. 1, the co- and contrahanded intensity reflectances for an extreme value of chirality, $\alpha = -1.5\mathrm{Re}(\bar{n})$, are illustrated in Fig. 4. Evidently, for a particular set of parameters, two resonances arise: one, regular, for RCP light at $\lambda_0^{\rm Br}|_{\rm RH}^{\rm RCP} = 1.29\,\mu$m and one, reverse, for LCP light at $\lambda_0^{\rm Br}|_{\rm RH}^{\rm LCP} = 259.55$ nm. The relevant intensity transmittances are illustrated in Fig. 5, where the envelope behavior is associated with increased absorption for increased optical thickness. The peculiar response at the wavelength lying exactly between the two resonances is discussed in Sec. V.

The requirement $|\alpha| > \mathrm{Re}(\bar{n})$ signifies extreme values of chirality, equivalent to a rotation of the electric field vector within a wavelength in the medium. This has been identified in Refs. [32,33] as the negative refraction due to the chirality regime, and in Ref. [44], modes with negative phase velocity in isotropic chiral media were demonstrated. This is fundamentally distinct from the handedness reversal phenomenon of Ref. [38], where both the permittivity and permeability of a structurally chiral medium were taken to be negative. Accessing such large values of chirality has been achieved in metamaterials at terahertz [34], gigahertz [35,36], and optical frequencies [45], without, however, requiring the permittivity and permeability to be *simultaneously* negative. Regarding the visible spectrum, varying the conductivity, as done in

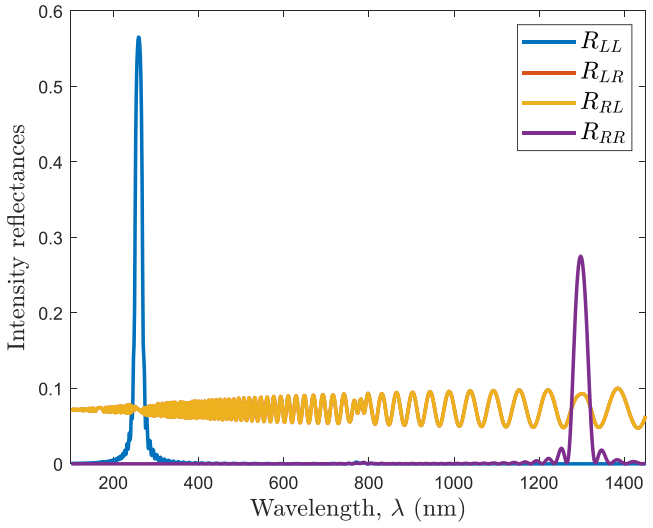

FIG. 4. Intensity reflectances of the setup in Fig. 1 for an extreme value of chirality, $\alpha = -1.5\mathrm{Re}(\bar{n})$. The contrahanded reflectances R_{LR} and R_{RL} coincide.

Ref. [46], provides the necessary tunability for switching operations. We note, however, that for $\bar{n} \approx \pm\alpha$, the credibility of the Drude-Born-Fedorov model is questioned [47]. The existence of these remarkable resonances is further confirmed via coupled wave theory in Appendix B, where the rigorous analysis is significantly simplified.

V. CIRCULAR BIREFRINGENCE OFFSETTING STRUCTURAL CHIRALITY

A further interesting observation can be made on Eq. (14). In fact, when $k_0\alpha = -hp$ (N.B. α can take either sign), or in terms of wavelength at

$$\lambda_0^c \underset{h=+1}{=} \tfrac{1}{2}\left(\lambda_0^{\mathrm{Br}}\big|_{\mathrm{RH}}^{\mathrm{LCP}} + \lambda_0^{\mathrm{Br}}\big|_{\mathrm{RH}}^{\mathrm{RCP}}\right) = -L_p\alpha$$
$$\underset{h=-1}{=} \tfrac{1}{2}\left(\lambda_0^{\mathrm{Br}}\big|_{\mathrm{LH}}^{\mathrm{LCP}} + \lambda_0^{\mathrm{Br}}\big|_{\mathrm{LH}}^{\mathrm{RCP}}\right) = L_p\alpha, \tag{26}$$

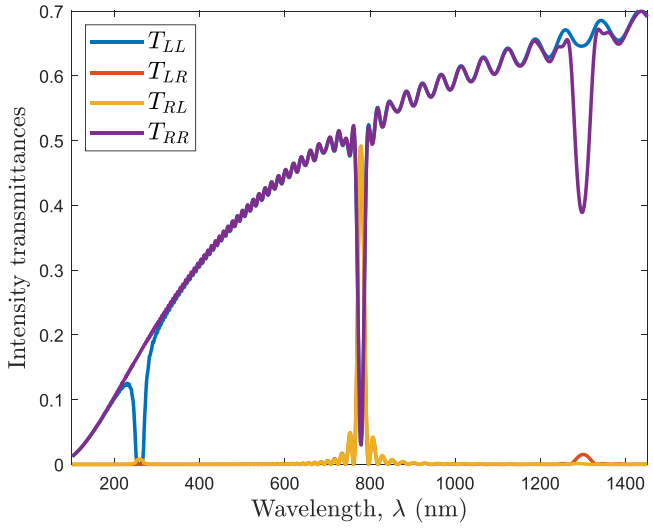

FIG. 5. Intensity transmittances for the scenario of Fig. 4.

which lies exactly in between the two resonances of Fig. 5 and is equal to the chirality-induced spectral shift, circular birefringence *precisely offsets* structural chirality. At this wavelength, the fields $\mathbf{e}$, $\mathbf{h}$, which are twisting along with the helix, experience a linearly birefringent medium. The forward propagating modes are then $\mathbf{e}_1 = (\exp(i\tilde{n}k_0 z),\ 0)^T$ and $\mathbf{e}_2 = (0,\ \exp(in_b k_0 z))^T$, where $\tilde{n} = (\tilde{\varepsilon}\mu)^{1/2}$ and $n_b = (\varepsilon_b\mu)^{1/2}$. When transformed back using Eqs. (11a) and (11b), we get

$$\mathbf{E}_1 = e^{i\tilde{n}k_0 z}\begin{pmatrix}\cos(pz)\\ h\sin(pz)\end{pmatrix}, \tag{27a}$$

$$\mathbf{E}_2 = e^{in_b k_0 z}\begin{pmatrix}-h\sin(pz)\\ \cos(pz)\end{pmatrix}, \tag{27b}$$

which correspond to linearly polarized fields, in Cartesian coordinates, that rotate with the eigenaxes of the structurally chiral medium. The total transverse field is

$$\mathbf{E}_\perp = A_1\mathbf{E}_1 + A_2\mathbf{E}_2, \tag{28}$$

where $A_{1,2}$ are the amplitudes of the electric fields. Interestingly, $\mathbf{E}_1$ and $\mathbf{E}_2$ are at once *orthogonal but cohanded*, taking the same chirality as the structurally chiral medium. Converting the expression in Eq. (28) to an equivalent in a circular basis, we obtain

$$\begin{pmatrix}E_L^+\\ E_R^+\end{pmatrix}_{z=L} = \mathbf{T}\begin{pmatrix}E_L^+\\ E_R^+\end{pmatrix}_{z=0}, \tag{29}$$

where

$$\mathbf{T} = \begin{pmatrix}e^{ik_0(\bar{n}+\alpha)z}\cos(k_0\tilde{\tilde{n}}z) & ie^{ik_0(\bar{n}+\alpha)z}\sin(k_0\tilde{\tilde{n}}z)\\ ie^{-ik_0(\bar{n}-\alpha)z}\sin(k_0\tilde{\tilde{n}}z) & e^{-ik_0(\bar{n}-\alpha)z}\cos(k_0\tilde{\tilde{n}}z)\end{pmatrix},$$

with $\tilde{\tilde{n}} = (\tilde{n} - n_b)/2$. This represents a continuous exchange between circular states as light propagates through a linearly birefringent medium, due to its unnatural expansion in a circular basis.

At λ_0^c, plotting the transmittances of Fig. 1, accessed via Eq. (29), as functions of the slab thickness in Fig. 6, we see that the energy between T_{LL} (T_{RR}) and T_{RL} (T_{LR}) is exchanged. In this regime, circular birefringence counteracts structural chirality, effectively "unwrapping" the medium, which light now sees as simply linearly birefringent with refractive indices $\tilde{n}$ and n_b. Moving towards shorter wavelengths, the medium is "wrapped" again but this time with an opposite handedness, so that a reverse circular Bragg phenomenon occurs.

VI. CONCLUSIONS

The axial propagation of circularly polarized light in circularly birefringent structurally chiral media was addressed via full electromagnetic analysis, and some underlying symmetries of the system's characteristic matrix led to additional resonances, previously unknown. For chirality comparable to the average refractive index, in the negative refraction regime, the handedness of the cohanded forward propagating mode swaps with the handedness of the contrahanded backward propagating one, bringing the latter into resonance. At another wavelength, lying exactly between the two resonances, circular birefringence exactly offsets structural chirality, rendering

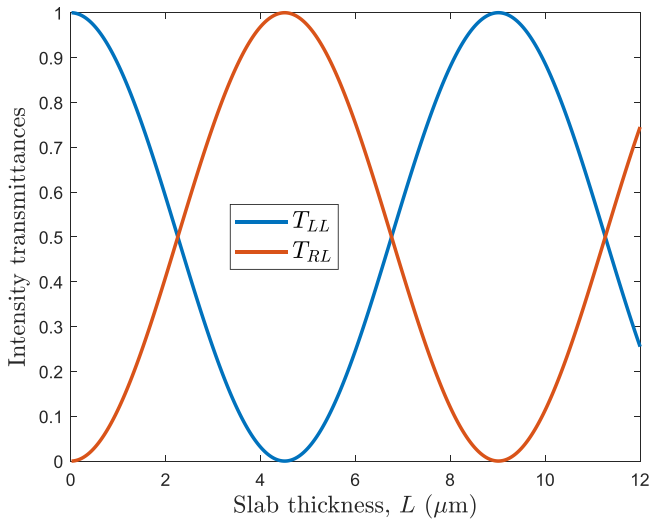

FIG. 6. Periodic exchange of circular states as a function of the slab thickness at λ_0^c (cf. Fig. 5) as per Eq. (29). The parameters are those of Fig. 1.

the medium simply linearly birefringent. There, circular polarizations degenerate to linear, orthogonal, and cohanded, rotating at the same rate as the structurally chiral medium's eigenaxes. Assessing the required parameter, we contend that they are accessible via current metamedia technology at terahertz, gigahertz, and optical frequencies. Applications in switching operations, modern optoelectronics, and sensing may be stimulated.

ACKNOWLEDGMENTS

The authors would like to acknowledge fruitful discussions with Dr. K. Weir of the Department of Physics at Imperial College London.

APPENDIX A: REVIEW OF CIRCULAR BIREFRINGENCE

The eigenvalues of the matrix $\mathbf{S}$ on the right-hand side of Eq. (10), for $\boldsymbol{\epsilon}_\perp$ reverted to ε, are $\lambda_\pm = -i(\alpha \pm \bar{n})$, each with multiplicity 2, with corresponding eigenvectors $\mathbf{u}_\pm = (\mathbf{v}, \mp i\mathbf{v}/\eta)^T$, where $\eta = (\mu/\varepsilon)^{1/2}$ and $\mathbf{v} \in \mathbb{C}^2$. Then,

$$\mathbf{D} = \begin{pmatrix} \lambda_+\mathbb{I} & \mathbf{0} \\ \mathbf{0} & \lambda_-\mathbb{I} \end{pmatrix} = \mathbf{U}^{-1} \cdot \mathbf{S} \cdot \mathbf{U},$$

where

$$\mathbf{U} = \begin{pmatrix} \mathbb{I} & \mathbb{I} \\ -i/\eta\mathbb{I} & i/\eta\mathbb{I} \end{pmatrix}.$$

For fields propagating along the z axis, with an $\exp(ikz)$ dependence, Eq. (10) is expressed as

$$k(\times)\begin{pmatrix} \mathbf{Q}_1 \\ \mathbf{Q}_2 \end{pmatrix} = \begin{pmatrix} -i\gamma_+\mathbb{I} & \mathbf{0} \\ \mathbf{0} & -i\gamma_-\mathbb{I} \end{pmatrix}\begin{pmatrix} \mathbf{Q}_1 \\ \mathbf{Q}_2 \end{pmatrix}, \tag{A1}$$

where $\gamma_\pm = k_0(\alpha \pm \bar{n})$ and the Beltrami fields are

$$\begin{pmatrix} \mathbf{Q}_1 \\ \mathbf{Q}_2 \end{pmatrix} = \mathbf{U}^{-1}\begin{pmatrix} \mathbf{E}_\perp \\ \mathbf{h}_\perp \end{pmatrix} = \frac{1}{2}\begin{pmatrix} \mathbf{E}_\perp + i\eta\mathbf{h}_\perp \\ \mathbf{E}_\perp - i\eta\mathbf{h}_\perp \end{pmatrix}.$$

Then, Eq. (A1) yields

$$\begin{pmatrix} i\gamma_+ & -k \\ k & i\gamma_+ \end{pmatrix}\begin{pmatrix} Q_{1x} \\ Q_{1y} \end{pmatrix} = 0,$$

with eigenvalues $k_{1\pm} = \pm\gamma_+$, and

$$\begin{pmatrix} i\gamma_- & -k \\ k & i\gamma_- \end{pmatrix}\begin{pmatrix} Q_{2x} \\ Q_{2y} \end{pmatrix} = 0,$$

with eigenvalues $k_{2\pm} = \pm\gamma_-$.

For $|\alpha| < \mathrm{Re}(\bar{n})$, the modes propagating along $+z$ have wave numbers k_{1+} and k_{2-}. The corresponding eigenvectors propagate according to

$$\mathbf{Q}_{1+} = Q_{1+}\frac{e^{ik_0(\bar{n}+\alpha)z}}{\sqrt{2}}\begin{pmatrix} 1 \\ i \end{pmatrix},$$

$$\mathbf{Q}_{2+} = Q_{2+}\frac{e^{ik_0(\bar{n}-\alpha)z}}{\sqrt{2}}\begin{pmatrix} 1 \\ -i \end{pmatrix},$$

where Q_{1+} and Q_{2+} are constants. If $Q_{2+} = 0$, then $\mathbf{E}_\perp = \mathbf{E}_{1+} = \mathbf{Q}_{1+}$, and we have

$$\mathrm{Re}(\mathbf{E}_{1+}) = \frac{|Q_{1+}|e^{-k_0\mathrm{Im}(\bar{n})z}}{\sqrt{2}}\begin{pmatrix} \cos[\mathrm{Re}(\gamma_+)z + \arg(Q_{1+})] \\ -\sin[\mathrm{Re}(\gamma_+)z + \arg(Q_{1+})] \end{pmatrix}, \tag{A2}$$

corresponding to an electric field that describes a left-handed helix in space. Similarly, if $Q_{1+} = 0$, then $\mathbf{E}_\perp = \mathbf{E}_{2+} = \mathbf{Q}_{2+}$ and

$$\mathrm{Re}(\mathbf{E}_{2+}) = \frac{|Q_{2+}|e^{-k_0\mathrm{Im}(\bar{n})z}}{\sqrt{2}}\begin{pmatrix} \cos[-\mathrm{Re}(\gamma_-)z + \arg(Q_{2+})] \\ \sin[-\mathrm{Re}(\gamma_-)z + \arg(Q_{2+})] \end{pmatrix}, \tag{A3}$$

corresponding to a field describing a right-handed helix in space. The modes propagating along $-z$ have wave numbers k_{1-} and k_{2+} with corresponding eigenvectors

$$\mathbf{Q}_{1-} = Q_{1-}\frac{e^{-ik_0(\bar{n}+\alpha)z}}{\sqrt{2}}\begin{pmatrix} 1 \\ i \end{pmatrix},$$

$$\mathbf{Q}_{2-} = Q_{2-}\frac{e^{-ik_0(\bar{n}-\alpha)z}}{\sqrt{2}}\begin{pmatrix} 1 \\ -i \end{pmatrix}.$$

The fields found by setting $Q_{2-} = 0$ and $Q_{1-} = 0$ are

$$\mathrm{Re}(\mathbf{E}_{1-}) = \frac{|Q_{1-}|e^{k_0\mathrm{Im}(\bar{n})z}}{\sqrt{2}}\begin{pmatrix} \cos[\mathrm{Re}(\gamma_+)z + \arg(Q_{1-})] \\ \sin[\mathrm{Re}(\gamma_+)z + \arg(Q_{1-})] \end{pmatrix}$$

and

$$\mathrm{Re}(\mathbf{E}_{2-}) = \frac{|Q_{2-}|e^{k_0\mathrm{Im}(\bar{n})z}}{\sqrt{2}}\begin{pmatrix} \cos[-\mathrm{Re}(\gamma_-)z + \arg(Q_{2-})] \\ -\sin[-\mathrm{Re}(\gamma_-)z + \arg(Q_{2-})] \end{pmatrix},$$

respectively.

When $\alpha > \mathrm{Re}(\bar{n})$ (respectively, $\alpha < -\mathrm{Re}(\bar{n})$), the direction of phase advance for $\mathbf{E}_{2+}$ ($\mathbf{E}_{1+}$) changes from being positive to being negative, so that $\mathbf{E}_{2+}$ ($\mathbf{E}_{1+}$) describes a wave whose phase propagates along $-z$. Moreover, $\mathrm{Re}(\mathbf{E}_{2+})$ ($\mathrm{Re}(\mathbf{E}_{1+})$) changes from describing a right-handed (left-handed) helix to a left-handed (right-handed) helix. Similarly, the direction of phase advance for $\mathbf{E}_{2-}$ ($\mathbf{E}_{1-}$) changes from being negative to being positive, so that $\mathbf{E}_{2-}$ ($\mathbf{E}_{1-}$) describes a wave whose phase propagates along $+z$ and $\mathrm{Re}(\mathbf{E}_{2-})$ ($\mathrm{Re}(\mathbf{E}_{1-})$) changes from describing a left-handed (right-handed) helix to a right-handed (left-handed) helix. While the

direction of phase propagation changes, the Poynting vector does not change [48].

APPENDIX B: COUPLED WAVE THEORY DESCRIPTION OF CIRCULAR BIREFRINGENCE WITH STRUCTURAL CHIRALITY

Reverting the tensor $\boldsymbol{\epsilon}$ to a scalar ε, Eq. (5) will be describing circular birefringence without structural chirality. The transverse electric field of plane waves is

$$\mathbf{E}_\perp = (A_L^+ e^{ik_0(\bar{n}+\alpha)z} + A_R^- e^{-ik_0(\bar{n}-\alpha)z})\mathbf{Q}_1 + (A_R^+ e^{ik_0(\bar{n}-\alpha)z} + A_L^- e^{-ik_0(\bar{n}+\alpha)z})\mathbf{Q}_2, \tag{B1}$$

in a circular basis, where

$$\mathbf{Q}_1 = \frac{1}{\sqrt{2}}\begin{pmatrix}1\\ i\end{pmatrix} \quad \text{and} \quad \mathbf{Q}_2 = \frac{1}{\sqrt{2}}\begin{pmatrix}1\\ -i\end{pmatrix}.$$

For $|\alpha| < \bar{n}$, the amplitudes of Eq. (B1) are appropriately notated, whereas for $|\alpha| > \bar{n}$, the phase velocity and handedness of some modes reverse; see Appendix A.

The amplitudes are assumed to be slowly varying functions of z. Substituting Eq. (B1), along with Eqs. (6), (7), and (9), into Eq. (5), retaining potentially phase-matched terms, and resolving along $\mathbf{Q}_1$ and $\mathbf{Q}_2$ yields

$$\frac{dA_L^+}{dz}e^{ik_0(\bar{n}+\alpha)z} - \frac{dA_R^-}{dz}e^{-ik_0(\bar{n}-\alpha)z} = i\kappa A_R^+ e^{i[k_0(\bar{n}-\alpha)-2hp]z} + i\kappa A_L^- e^{-i[k_0(\bar{n}+\alpha)+2hp]z} \tag{B2}$$

and

$$\frac{dA_R^+}{dz}e^{ik_0(\bar{n}-\alpha)z} - \frac{dA_L^-}{dz}e^{-ik_0(\bar{n}+\alpha)z} = i\kappa A_L^+ e^{i[k_0(\bar{n}+\alpha)+2hp]z} + i\kappa A_R^- e^{-i[k_0(\bar{n}-\alpha)-2hp]z}. \tag{B3}$$

The coupling constant is $\kappa = \pi\delta\bar{n}/\lambda_0$, where $\delta\bar{n} = |\tilde{n} - n_b|$ is the local linear birefringence. The absorption is almost constant over the range of $\delta\bar{n}$ so that $\kappa \in \mathbb{R}$.

For different phase-matching scenarios, Eqs. (B2) and (B3) can be distilled into

$$\frac{d}{dz}\begin{pmatrix}A_L^+\\ A_L^-\\ A_R^+\\ A_R^-\end{pmatrix} = \mathbf{K}\begin{pmatrix}A_L^+\\ A_L^-\\ A_R^+\\ A_R^-\end{pmatrix}, \tag{B4}$$

where

$$\mathbf{K} = i\kappa\begin{pmatrix}0 & e^{-i\delta_L z} & e^{-i\delta_c z} & 0\\ -e^{i\delta_L z} & 0 & 0 & -e^{i\delta_c z}\\ e^{i\delta_c z} & 0 & 0 & e^{-i\delta_R z}\\ 0 & -e^{-i\delta_c z} & -e^{i\delta_R z} & 0\end{pmatrix},$$

and the various detuning parameters are given by

$$\delta_R = 2k_0(\bar{n}-\alpha) - 2hp, \tag{B5a}$$

$$\delta_L = 2k_0(\bar{n}+\alpha) + 2hp, \tag{B5b}$$

$$\delta_c = 2k_0\alpha + 2hp. \tag{B5c}$$

For a right-handed medium, the on-resonance condition for RCP light, $\mathrm{Re}(\delta_R) = 0$, corroborates Eq. (17). For a left-handed medium the $\mathrm{Re}(\delta_L) = 0$ condition for LCP light corroborates Eq. (18). Finally, setting $\delta_c = 0$, we obtain $k_0\alpha = -hp$, corroborating Eq. (26) and corresponding to the modes given by Eqs. (27a) and (27b).

For each identified resonance, coupled wave theory provides a pair of readily solved equations from which the relevant z-dependent amplitudes are deduced. Then, the total transverse electric field may be reconstructed via Eq. (B1) so that the optical spectrum can be calculated as in Ref. [19]. For $\delta_{R,L} \approx 0$, the evolution of the amplitudes is given by the solutions to Eqs. (B4)

$$\begin{pmatrix}A_{R,L}^+\\ A_{\bar{R},L}^-\end{pmatrix}_{z=L} = \begin{pmatrix}p_{R,L}^+ & q_{R,L}^+\\ q_{R,L}^- & p_{\bar{R},L}^-\end{pmatrix}\begin{pmatrix}A_{R,L}^+\\ A_{\bar{R},L}^-\end{pmatrix}_{z=0},$$

where

$$p_{R,L}^\pm(z) = e^{\mp\frac{i\delta_{R,L}}{2}z}\left[\cosh(\Delta_{R,L}z) \pm i\frac{\delta_{R,L}}{2\Delta_{R,L}}\sinh(\Delta_{R,L}z)\right],$$

$$q_{R,L}^\pm(z) = \pm ie^{\mp\frac{i\delta_{R,L}}{2}z}\frac{\kappa}{\Delta_{R,L}}\sinh(\Delta_{R,L}z),$$

with $\Delta_{R,L} = [\kappa^2 - (\delta_{R,L}/2)^2]^{1/2}$.

For $\delta_c \approx 0$, the solution is slightly different. In fact,

$$\begin{pmatrix}A_L^+\\ A_R^+\end{pmatrix}_{z=L} = \begin{pmatrix}\tilde{p}^+ & \tilde{q}\\ \tilde{q} & \tilde{p}^-\end{pmatrix}\begin{pmatrix}A_L^+\\ A_R^+\end{pmatrix}_{z=0},$$

where

$$\tilde{p}^\pm(z) = e^{\mp i\frac{\delta_c}{2}z}\left[\cos(\Delta_c z) \pm i\frac{\delta_c}{2\Delta_c}\sin(\Delta_c z)\right],$$

$$\tilde{q}(z) = ie^{\mp i\frac{\delta_c}{2}z}\frac{\kappa}{\Delta_c}\sin(\Delta_c z),$$

with $\Delta_c = [\kappa^2 + (\delta_c/2)^2]^{1/2}$. The circular components of the forward propagating electric fields are then

$$\begin{pmatrix}E_L^+\\ E_R^+\end{pmatrix}_{z=L} = e^{ik_0\bar{n}z}\begin{pmatrix}e^{-ihpz}\tilde{p}^+ & e^{-ihpz}\tilde{q}\\ e^{ihpz}\tilde{q} & e^{ihpz}\tilde{p}^-\end{pmatrix}\begin{pmatrix}E_L^+\\ E_R^+\end{pmatrix}_{z=0}. \tag{B6}$$

On noting that $2\kappa = k_0(\tilde{n} - n_b)$ and applying the condition $k_0\alpha = -hp$, the on-resonance ($\delta_c = 0$) representation of Eq. (B6) coincides with Eq. (29). In this instance, coupled wave theory, despite being an approximate method, yields the exact result.

Examining the on-resonance approximate expression for the peak reflectance, $R^{\mathrm{peak}} = \tanh^2(\kappa L)$ and for a particular handedness, say, right, for RCP, we have $k_0^R = p/(\bar{n} - a)$, while for LCP, $k_0^L = -p/(\bar{n} + a)$. Then,

$$R_{RR}^{\mathrm{peak}} = \tanh^2\left(\frac{p}{\bar{n}-\alpha}\frac{\mu\delta\varepsilon}{2\bar{n}}L\right), \tag{B7}$$

where it is evident that increasing α increases R_{RR}^{peak}. In contrast, for a left-handed medium, increasing α has the opposite impact on R_{LL}^{peak}. Therefore Eq. (B7) clearly demonstrates the monotonic relationship of R_{RR}^{peak} with α.

Finally, as seen in Ref. [28], circular birefringence also affects the resonance bandwidth. This can be estimated as $\Delta\lambda_0 = \mathrm{Re}(\delta\bar{n})L_p$. Considering that the optical rotation is roughly proportional to the square of $\delta\bar{n}$ [27], we have $\Delta\lambda_0 \sim \alpha^2 L_p$, explaining the quadratic behavior found in Ref. [28].

[1] A. A. Michelson, On metallic colouring in birds and insects, London Edinburgh Dublin Philos. Mag. J. Sci. **21**, 554 (1911).

[2] L. Kang, S. Lan, Y. Cui, S. P. Rodrigues, Y. Liu, D. H. Werner, and W. Cai, An active metamaterial platform for chiral responsive optoelectronics, Adv. Mater. **27**, 4377 (2015).

[3] S. Yoo and Q-H. Park, Metamaterials and chiral sensing: a review of fundamentals and applications, Nanophotonics **8**, 249 (2019).

[4] L. D. Barron, Molecular scattering of polarized light, in *Molecular Light Scattering and Optical Activity* (Cambridge University Press, Cambridge, 2009), Chap. 3, p. 163.

[5] G. Lakhwani and S. C. J. Meskers, Insights from chiral polyfluorene on the unification of molecular exciton and cholesteric liquid crystal theories for chiroptical phenomena, J. Phys. Chem. A **116**, 1121 (2012).

[6] K. Robbie, M. J. Brett, and A. Lakhtakia, Chiral sculptured thin films, Nature (London) **384**, 616 (1996).

[7] O. Arteaga, Natural optical activity vs circular Bragg reflection studied by Mueller matrix ellipsometry, Thin Solid Films **617**, 14 (2016).

[8] J. Wade, J. N. Hilfiker, J. R. Brandt, L. Liirò-Peluso, L. Wan, X. Shi, F. Salerno, S. T. J. Ryan, S. Schöeche, O. Arteaga, T. Jávorfi, G. Siligardi, C. Wang, D. B. Amabilino, P. H. Beton, A. J. Campbell, and M. J. Fuchter, Natural optical activity as the origin of the large chiroptical properties in π-conjugated polymer thin films, Nat. Commun. **11**, 6137 (2020).

[9] J. M. Han, S. Guo, H. Lu, S. Liu, Q. Zhao, and W. Huang, Recent progress on circularly polarized luminescent materials for organic optoelectronic devices, Adv. Opt. Mater. **6**, 1800538 (2018).

[10] T.-Y. Li, Y.-M. Jing, X. Liu, Y. Zhao, L. Shi, Z. Tang, Y.-X. Zheng, and J.-L. Zuo, Circularly polarised phosphorescent photoluminescence and electroluminescence of iridium complexes, Sci. Rep. **5**, 14912 (2015).

[11] Y. Yang, R. C. da Costa, M. J. Fuchter, and A. J. Campbell, Circularly polarized light detection by a chiral organic semiconductor transistor, Nat. Photonics **7**, 634 (2013).

[12] A. Lininger, G. Palermo, A. Guglielmelli, G. Nicoletta, M. Goel, M. Hinczewski, and G. Strangi, Chirality in light-matter interaction, Adv. Mater. 2107325 (2022).

[13] C. Wang, Z. Li, R. Pan, W. Liu, H. Cheng, J. Li, W. Zhou, J. Tian, and S. Chen, Giant intrinsic chirality in curled metasurfaces, ACS Photonics **7**, 3415 (2020).

[14] G. Long, G. Adamo, J. Tian, M. Klein, H. N. S. Krishnamoorthy, E. Feltri, H. Wang, and C. Soci, Perovskite metasurfaces with large superstructural chirality, Nat. Commun. **13**, 1551 (2022).

[15] M. W. McCall and A. Lakhtakia, Development and assessment of coupled wave theory of axial propagation in thin-film helicoidal bianisotropic media. Part 1: Reflectances and transmittances, J. Mod. Opt. **47**, 973 (2000).

[16] M. W. McCall and A. Lakhtakia, Development and assessment of coupled wave theory of axial propagation in thin-film helicoidal bi-anisotropic media. Part 2: Dichroisms, ellipticity transformation and optical rotation, J. Mod. Opt. **48**, 143 (2001).

[17] M. W. McCall and A. Lakhtakia, Explicit expressions for spectral remittances of axially excited chiral sculptured thin films, J. Mod. Opt. **51**, 111 (2004).

[18] A. Lakhtakia and R. Messier, *Sculptured Thin Films: Nanoengineered Morphology and Optics* (SPIE, Bellingham, WA, 2005).

[19] M. W. McCall, Simplified theory of axial propagation through structurally chiral media, J. Opt. A **11**, 074006 (2009).

[20] T. G. Mackay and A. Lakhtakia, On the theory of optical sensing via infiltration of sculptured thin films, in *Nanostructured Thin Films III*, Proceedings of SPIE Vol. 7766 (SPIE, Bellingham, WA, 2010), p. 77660O.

[21] A. Lakhtakia, On percolation and circular Bragg phenomenon in metallic, helicoidally periodic, sculptured thin films, Microw. Opt. Technol. Lett. **24**, 239 (2000).

[22] J. B. Sorge, A. C. van Popta, J. C. Sit, and M. J. Brett, Circular birefringence dependence on chiral film porosity, Opt. Express **14**, 10550 (2006).

[23] S. Shirin, A. Madani, and S. R. Entezar, Tunable lateral shift of the reflected optical beams from a nanocomposite structurally chiral medium, Opt. Mater. **107**, 110026 (2020).

[24] S. M. Pursel, M. W. Horn, and A. Lakhtakia, Blue-shifting of circular Bragg phenomenon by annealing of chiral sculptured thin films, Opt. Express **14**, 8001 (2006).

[25] T. G. Mackay and A. Lakhtakia, Empirical model of optical sensing via spectral shift of circular Bragg phenomenon, IEEE Photonics J. **2**, 92 (2010).

[26] A. Lakhtakia, Enhancement of optical activity of chiral sculptured thin films by suitable infiltration of void regions, Optik **112**, 145 (2001).

[27] I. Hodgkinson, Q. h. Wu, B. Knight, A. Lakhtakia, and K. Robbie, Vacuum deposition of chiral sculptured thin films with high optical activity, Appl. Opt. **39**, 642 (2000).

[28] J. A. Sherwin and A. Lakhtakia, Nominal model for the optical response of a chiral sculptured thin film infiltrated with an isotropic chiral fluid, Opt. Commun. **214**, 231 (2002).

[29] J. A. Sherwin and A. Lakhtakia, Nominal model for the optical response of a chiral sculptured thin film infiltrated by an isotropic chiral fluid-oblique incidence, Opt. Commun. **222**, 305 (2003).

[30] I. J. Hodgkinson, A. Lakhtakia, Q. h. Wu, L. De Silva, and M. W. McCall, Ambichiral, equichiral and finely chiral layered structures, Opt. Commun. **239**, 353 (2004).

[31] A. C. van Popta, M. J. Brett, and J. C. Sit, Double-handed circular Bragg phenomena in polygonal helix thin films, J. Appl. Phys. **98**, 083517 (2005).

[32] J. B. Pendry, A chiral route to negative refraction, Science **306**, 1353 (2004).

[33] C. Monzon and D. W. Forester, Negative Refraction and Focusing of Circularly Polarized Waves in Optically Active Media, Phys. Rev. Lett. **95**, 123904 (2005).

[34] S. Zhang, Y.-S. Park, J. Li, X. Lu, W. Zhang, and X. Zhang, Negative Refractive Index in Chiral Metamaterials, Phys. Rev. Lett. **102**, 023901 (2009).

[35] J. Zhou, J. Dong, B. Wang, T. Koschny, M. Kafesaki, and C. M. Soukoulis, Negative refractive index due to chirality, Phys. Rev. B **79**, 121104(R) (2009).

[36] E. Plum, J. Zhou, J. Dong, V. A. Fedotov, T. Koschny, C. M. Soukoulis, and N. I. Zheludev, Metamaterial with negative index due to chirality, Phys. Rev. B **79**, 035407 (2009).

[37] D. Zarifi, M. Soleimani, and V. Nayyeri, Dual-and multiband chiral metamaterial structures with strong optical activity and

negative refraction index, IEEE Antennas Wireless Propag. Lett. **11**, 334 (2012).

[38] A. Lakhtakia, Handedness reversal of circular Bragg phenomenon due to negative real permittivity and permeability, Opt. Express **11**, 716 (2003).

[39] Y. Wen, M.-Q. He, Y.-L. Yu, and J.-H. Wang, Biomolecule-mediated chiral nanostructures: a review of chiral mechanism and application, Adv. Colloid Interface Sci. **289**, 102376 (2021).

[40] C. F. Bohren, Isotropic chiral materials, in *Introduction to Complex Mediums for Optics and Electromagnetics*, edited by W. S. Weiglhofer and A. Lakhtakia, SPIE Press Monograph Series Vol. 123 (SPIE, Bellingham, WA, 2003), Chap. 3, p. 63–78.

[41] C. W. Oseen, The theory of liquid crystals, Trans. Faraday Soc. **29**, 883 (1933).

[42] M. W. McCall, I. Hodgkinson, and Q. Wu, Continuum methods, in *Birefringent Thin Films and Polarizing Elements* (Imperial College Press, London, 2015), Chap. 10, pp. 195–215.

[43] R. Mohammadi-Baghaee and J. Rashed-Mohassel, The chirality parameter for chiral chemical solutions, J. Solution Chem. **45**, 1171 (2016).

[44] T. G. Mackay, Plane waves with negative phase velocity in isotropic chiral mediums, Microwave Opt. Technol. Lett. **45**, 120 (2005).

[45] A. Y. Zhu, W. T. Chen, A. Zaidi, Y.-W. Huang, M. Khorasaninejad, V. Sanjeev, C.-W. Qiu, and F. Capasso, Giant intrinsic chiro-optical activity in planar dielectric nanostructures, Light Sci. Appl. **7**, 17158 (2018).

[46] M. Liu, E. Plum, H. Li, S. Li, Q. Xu, X. Zhang, C. Zhang, C. Zou, B. Jin, J. Han, and W. Zhang, Temperature-controlled optical activity and negative refractive index, Adv. Funct. Mater. **31**, 2010249 (2021).

[47] K. Cho, Dispersion relation in chiral media: Credibility of Drude-Born-Fedorov equations, in *Electromagnetic Metamaterials* (Springer, New York, 2019), Chap. 12, pp. 189–199.

[48] M. W. McCall, What is negative refraction? J. Mod. Opt. **56**, 1727 (2009).